How to cite: *Angew. Chem. Int. Ed.* **2023,** *62,* e202216633
International Edition: doi.org/10.1002/anie.202216633
German Edition: doi.org/10.1002/ange.202216633

Spectroelectrochemistry

Spectroscopy vs. Electrochemistry: Catalyst Layer Thickness Effects on Operando/In Situ Measurements

Justus S. Diercks, Juan Herranz, Kathrin Ebner, Nataša Diklić, Maximilian Georgi, Piyush Chauhan, Adam H. Clark, Maarten Nachtegaal, Alexander Eychmüller, and Thomas J. Schmidt*

Abstract: In recent years, operando/in situ X-ray absorption spectroscopy (XAS) has become an important tool in the electrocatalysis community. However, the high catalyst loadings often required to acquire XA-spectra with a satisfactory signal-to-noise ratio frequently imply the use of thick catalyst layers (CLs) with large ion- and mass-transport limitations. To shed light on the impact of this variable on the spectro-electrochemical results, in this study we investigate Pd-hydride formation in carbon-supported Pd-nanoparticles (Pd/C) and an unsupported Pd-aerogel with similar Pd surface areas but drastically different morphologies and electrode packing densities. Our in situ XAS and rotating disk electrode (RDE) measurements with different loadings unveil that the CL-thickness largely determines the hydride formation trends inferred from spectro-electrochemical experiments, therewith calling for the minimization of the CL-thickness in such experiments and the use of complementary thin-film control measurements.

The ongoing decarbonization of the energy sector heavily relies on the up-scaled deployment of electrochemical energy storage and conversion technologies (i.e., batteries, fuel cells and (co-)electrolyzers) that often implement active components based on scarce and/or expensive materials (e.g., Ir, Pt, Co).[1] The required decrease in the loading of these critical materials (or their substitution with abundant alternatives) is guided by an improved understanding of their properties under operative conditions that has been fostered by the increasingly common use of in situ/operando characterization techniques.[2] Among these, X-ray absorption spectroscopy (XAS) is particularly well suited for the study of fuel cell,[3] electrolyzer[2c,4] and CO_2-reduction electrocatalysts.[3d,4c,5] A common feature of these reactions is that they imply the consumption and/or evolution of gaseous species (i.e., H_2, O_2, CO_2 and/or CO) and that the materials of interest are often (spectro-)electrochemically studied in aqueous media, rather than in the polymer electrolyte, humidified-gas-fed cells envisaged for commercial applications.[6] Notably, such liquid electrolyte cells frequently display poor convection properties when compared to gas-fed devices or the rotating disk electrodes (RDEs) used by many laboratories for electrocatalyst characterization and performance benchmarking.[6b,7] This aspect is particularly critical when studying reactions entailing the consumption of gases dissolved in the electrolyte, since the subsequent buildup of reactant concentration gradients can influence the catalytic activity[8] and (in the case of the CO_2-reduction reaction, CO_2RR) product selectivity.[6c,9] Conversely, when studying gas-evolving reactions, the accumulation of bubbles within the CL-pores can lead to a localized loss of potential control[5i,10] and therewith influence the reliability of electrochemical and spectroscopic results.

These effects can be aggravated when working with highly loaded, thick electrodes like the ones commonly used for in situ XAS studies. Specifically, such measurements are often carried out in a transmission mode detection configuration requiring high catalyst loadings (often $\geq 1\ mg_{catalyst}\,cm^{-2}_{geo}$) that can translate into $\gg 1$ µm thick catalyst layers.[3a] This is in contrast with the lower loadings typically used in the actual electrochemical devices (e.g., in fuel cells or electrolyzers, $\leq 1\ mg_{catalyst}\,cm^{-2}_{geo}$) or in thin film

[*] Dr. J. S. Diercks, Dr. J. Herranz, Dr. K. Ebner, Dr. N. Diklić, P. Chauhan, Prof. Dr. T. J. Schmidt
Electrochemistry Laboratory, Paul Scherrer Institute
5232 Villigen-PSI (Switzerland)
E-mail: juan.herranz@psi.ch

Dr. M. Georgi, Prof. Dr. A. Eychmüller
Physical Chemistry, TU Dresden
01062 Dresden (Germany)

Dr. A. H. Clark, Dr. M. Nachtegaal
Laboratory for Synchrotron Radiation and Femtochemistry, Paul Scherrer Institute
5232 Villigen-PSI (Switzerland)

Prof. Dr. T. J. Schmidt
Laboratory of Physical Chemistry, ETH Zürich
8093 Zürich (Switzerland)

(TF−) RDE tests, which typically entail loadings ≪ 0.1 $mg_{catalyst}\,cm^{-2}_{geo}$.[11] Despite this, electrochemical and spectroscopic results acquired with very different catalyst loadings (i.e., individually optimized for each technique) are often compared while overlooking the possible influence of this variable and the corresponding layer thickness on the achieved results.[4b,12] This becomes particularly relevant with the ongoing upsurge of time-resolved operando/in situ XAS electrochemistry studies,[5i,13] for which the derived time-dependent results may be affected by the diffusion limitations discussed above.

To shed light on this plausible effect of the CL-thickness on time-resolved spectro-electrochemical results, in this work we studied the potential- and time-dependent formation of palladium hydride (PdH_x) using in situ XAS and RDE measurements with different catalyst loadings. We chose this PdH_x-formation process as a probe reaction because the concomitant increase of the Pd–Pd bonding distance quantifiable by XAS can be used to infer the hydride stoichiometry (i.e., the "x" in PdH_x),[3c,14] which can be complementarily estimated through electrochemical measurements based on the charge associated with the electro-oxidation of bulk-absorbed hydrogen.[3c,15] Additionally, the hydride-formation process is of great relevance for such key electrochemical reactions as the oxidation/evolution of H_2 or the reduction of CO_2 on Pd-catalysts, and has therefore been the subject of numerous spectro-electrochemical studies[3c,5b–f,15,16] entailing a large variety of measurement approaches and catalyst loadings (and corresponding CL-thicknesses) that we have summarized in Table S1.

To enable this investigation, we chose to perform these measurements on a commercial, 40 wt.-% Pd-on-carbon (Pd/C) catalyst and an unsupported Pd-aerogel synthesized based on an established ethanolic synthesis route[17] and previously extensively characterized and tested for CO_2-electroreduction.[16c] Notably, both of these materials feature similar nanostructure sizes and corresponding electrochemical surface areas (ECSAs—i.e., a mean nanoparticle size vs. an average web thickness of ≈5 vs. ≈6 nm and ECSAs of ≈50 vs. ≈40 $m^2\,g^{-1}$ for Pd/C vs. the Pd-aerogel, respectively).[18] However, the same two materials feature a ≈5-fold difference in effective packing densities (compare Table 1) that allowed us to produce electrodes with similar Pd-loadings but drastically different CL-thicknesses. Furthermore, we carried out these measurements in a N_2-saturated phosphate buffer with a pH of 7.3 (similar to that of many CO_2-saturated bicarbonate solutions used for CO_2-electroreduction studies)[19] devoid of gaseous reactants and within a narrow potential window (between −100 and 100 mV vs. the reversible hydrogen electrode (RHE)). Thus, these measurement conditions should minimize the impact of limitations in reactant-availability and/or product- (i.e., bubble) evacuation discussed above on the results reported in what follows.

We started our study by assessing hydride formation in the two materials using in situ XAS during a series of 10 min long potential holds. For these transmission XAS measurements, we used Pd-loadings of ≈3 vs. ≈1 $mg_{Pd}\,cm^{-2}_{geo}$ for Pd/C vs. the Pd-aerogel, which led to CL-thicknesses of ≈60 μm vs. ≈5 μm, respectively (see Table 1). The PdH_x-stoichiometries at the end of each potential hold are plotted in Figure 1a, and were calculated from the lattice expansion (Figure S1) derived from the fits of the Fourier-transformed extended X-ray absorption fine structure (EXAFS) spectra (see Figures S2 and S3 and the fitting parameters listed in Tables S2 and S3) using a method previously presented[3c,14,19a] and described in the experimental section. In agreement with previous studies,[3c,15,16b,19a,20] both Pd-based materials remain in the fully metallic form down to a potential of 0.1 V vs. the reversible hydrogen electrode (V_{RHE}). Further decreasing the potential leads to a sudden onset of hydride formation that is completed (yielding the so-called β-PdH_x-phase) at differing potentials of ≈0.05 vs. ≈0 V_{RHE} for the Pd-aerogel vs. Pd/C, respectively.

To gain more insight into the time-dependency of this hydride-formation process, the time-resolved X-ray absorption near-edge structure (XANES) spectra acquired at each potential were fitted through a linear combination fit (LCF) approach using the spectra acquired at the end of the 400 and −100 mV_{RHE} holds (displayed in Figure S4) as representative of metallic Pd vs. β-PdH_x, respectively. For this, the XANES-spectra acquired in the course of each potential hold were divided into groups of 10 spectra, averaged, and LC-fitted to yield the time-resolved PdH_x-contents in Figures 1b and c (for which the corresponding lacks-of-fit are featured in Figure S5). These time-dependent results show that the rates of hydride formation largely differ between both catalysts, whereby even at a potential of 0 V_{RHE} entailing the complete formation of the hydride, this process requires ≈300 vs. ≈550 s for the Pd-aerogel vs. Pd/C. Additionally, this time-resolved analysis unveils that, for the Pd/C sample, the formation of the PdH_x-phase at 50 mV_{RHE} is still in progress by the end of the 10 min potential hold; as such, the discrepancies in the potentials of complete hydride formation discussed above and displayed in Figure 1a may not be caused by intrinsic differences among these materials, but stem from an insufficient measurement time in the case of the Pd/C catalyst.

Table 1: Summary of the loadings and estimated catalyst layer thicknesses of the Pd/C and Pd-aerogel electrodes employed in our RDE and XAS measurements.

		Pd-loading [$\mu g_{Pd}\,cm^{-2}_{geo}$]	Electrode thickness[a] [μm]
Pd/C	RDE	10	≈0.2
		50	≈1.0
		500	≈10
	XAS	≈3000	≈60
Pd-aerogel	RDE	50	≈0.2
		500	≈2.3
	XAS	≈1000	≈4.7

[a] Estimated considering densities of 12 $g\,cm^{-3}$ for Pd[21] and 2 $g\,cm^{-3}$ for the carbon support,[21] Nafion® ionomer-to-metal and -to-carbon mass ratios of 0.3 vs. 0.2 for the Pd-aerogel vs. Pd/C, respectively (see the experimental section for details), and assuming a CL-porosity of ≈50% along with a negligible contribution of the Pd-nanoparticles in Pd/C to the corresponding CL-thickness/-volume.[22]

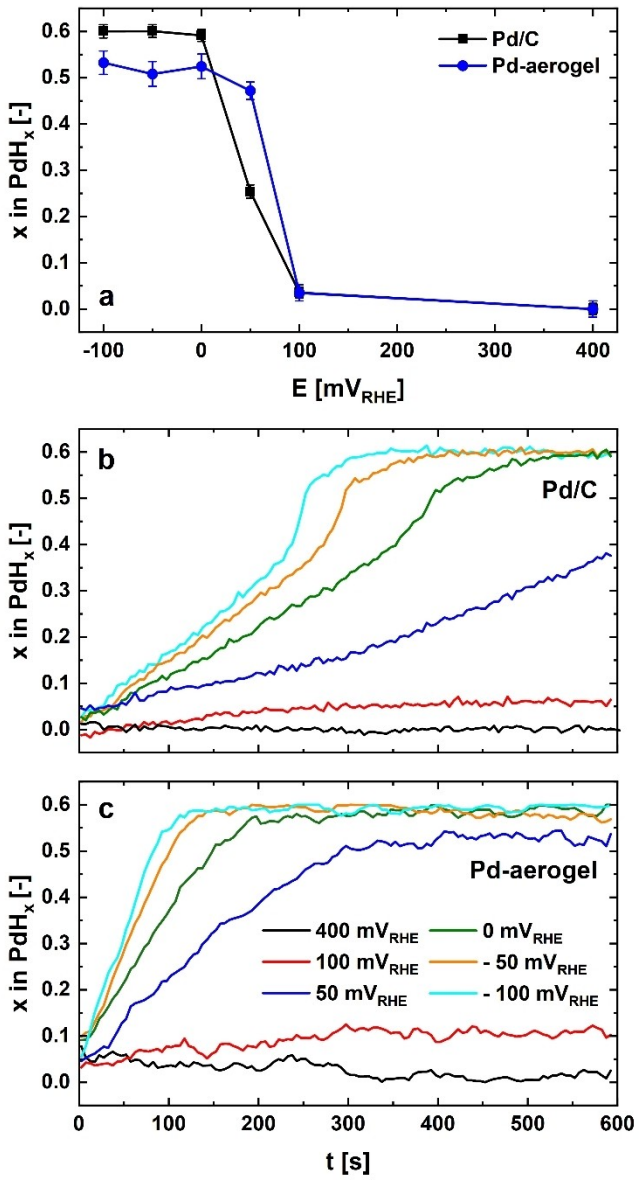

Figure 1. Potential-dependent Pd-hydride stoichiometries at the end of the 10-minute potential holds derived from the fits of the corresponding EXAFS-spectra (a) and time-resolved β-PdH$_x$ contents derived from the linear combination fits (LCFs) of the corresponding XANES-spectra acquired at the given potentials for Pd/C (b) and the Pd-aerogel (c). Note that the time-resolved hydride content values reported for the Pd-aerogel in "c" were smoothed by applying a floating average over 5 points.

To investigate the possible effect of the CLs' thickness on these XAS-derived hydride-formation trends, we performed additional RDE measurements on both catalysts using Pd-loadings of ≈50 vs. ≈500 $\mu g_{Pd}\,cm^{-2}_{geo}$, whereby the latter is set to be as close as possible to the loadings used for in situ XAS (leading to a ≈10 µm thick Pd/C CL) and the former results in layers within the (sub)micrometer range for both materials (see Table 1). Complementarily, the Pd/C catalyst was also measured using a loading of 10 $\mu g_{Pd}\,cm^{-2}_{geo}$, to match the ≪1 µm CL-thickness of the thinner Pd-aerogel layer (i.e., ≈0.2 µm—cf. Table 1).

The resulting linear sweep voltammograms (LSVs) used to oxidize (i.e., de-load) absorbed hydrogen after 1 min holds at the specified potentials are displayed in Figure 2a–d, and their oxidation charges used to estimate the corresponding PdH$_x$-stoichiometries are plotted in Figure 2e–f (see Supporting Information Note 1 and Figure S6 in the Supporting Information for details on the procedures of hydride-content quantification). Interestingly, the PdH$_x$-stoichiometries inferred for the Pd/C catalyst using this electrochemical approach significantly vary as a function of the catalyst loading, whereby the low loading, 50 $\mu g_{Pd}\,cm^{-2}_{geo}$ electrode (Figure 2a) features large and overlapping hydride-oxidation currents for all potential holds <50 mV$_{RHE}$ and no significant hydride oxidation at potentials >50 mV$_{RHE}$. Notably, this transition from metallic Pd to β-PdH$_x$ within a narrow potential window is perfectly reproduced when the loading (and corresponding CL-thickness) is further reduced to 10 $\mu g_{Pd}\,cm^{-2}_{geo}$ (see Figures S7a and S8a) indicating that no layer thickness effects apply for CLs ≤ 1 µm in thickness. To analyze the nature of the transition (i.e., equilibrium stoichiometry vs. unfinished formation of PdH) at 50 mV$_{RHE}$, the hydride oxidation peak dependence on the holding time was investigated (Figure S7b) and the stoichiometries extracted from the charges were plotted over time (Figure S7c). Here, the charge increases at low holding times (i.e., 1 to 30 s) and it becomes constant between 60 and 300 s, hence indicating that the hydride stoichiometry presented above on Pd/C at 50 mV$_{RHE}$ represents an equilibrium stoichiometry at PdH$_{\approx 0.3}$ (i.e., a mixed α-/β-hydride phase).

On the other hand, when the electrode loading is increased to 500 $\mu g_{Pd}\,cm^{-2}_{geo}$ (Figure 2c), a much slower increase in the hydride oxidation currents is observed when the potential hold values are decreased, with overlapping hydride-oxidation currents only appearing after potential holds below 12.5 mV$_{RHE}$. This attainment of the maximum stoichiometry at higher overpotentials (Figure 2e) can be linked to a slowed PdH$_x$-formation in the specific case of the highly-loaded Pd/C electrode, which would agree with the delayed PdH$_x$-formation kinetics (compared with the Pd-aerogel) inferred from our in situ XAS measurements (see the discussion above and Figure 1b vs. c). Additionally, the baseline cyclic voltammogram (CV) recorded at this higher loading (Figure S2c) differs significantly from the ones measured with 50 (Figure 2a) or 10 $\mu g_{Pd}\,cm^{-2}_{geo}$ (Figure S7a,b), with its overlapping voltammetric features related to Pd-(hydr)oxide formation/reduction and hydrogen ad-/desorption indicating a significant delay in these pseudo-capacitive processes.

Contrarily, the linear potential sweeps recorded on the Pd-aerogel at both loadings (see Figures 2b and d, along with the PdH$_x$-stoichiometries in Figure 2f) display a continuous increase in the hydride oxidation charge over a broad potential range extending from ≈50 to ≈−50 mV$_{RHE}$. While this similarity between the results derived from measurements with 10-fold different loadings may appear striking, one has to consider that the 500 $\mu g_{Pd}\,cm^{-2}_{geo}$ Pd-

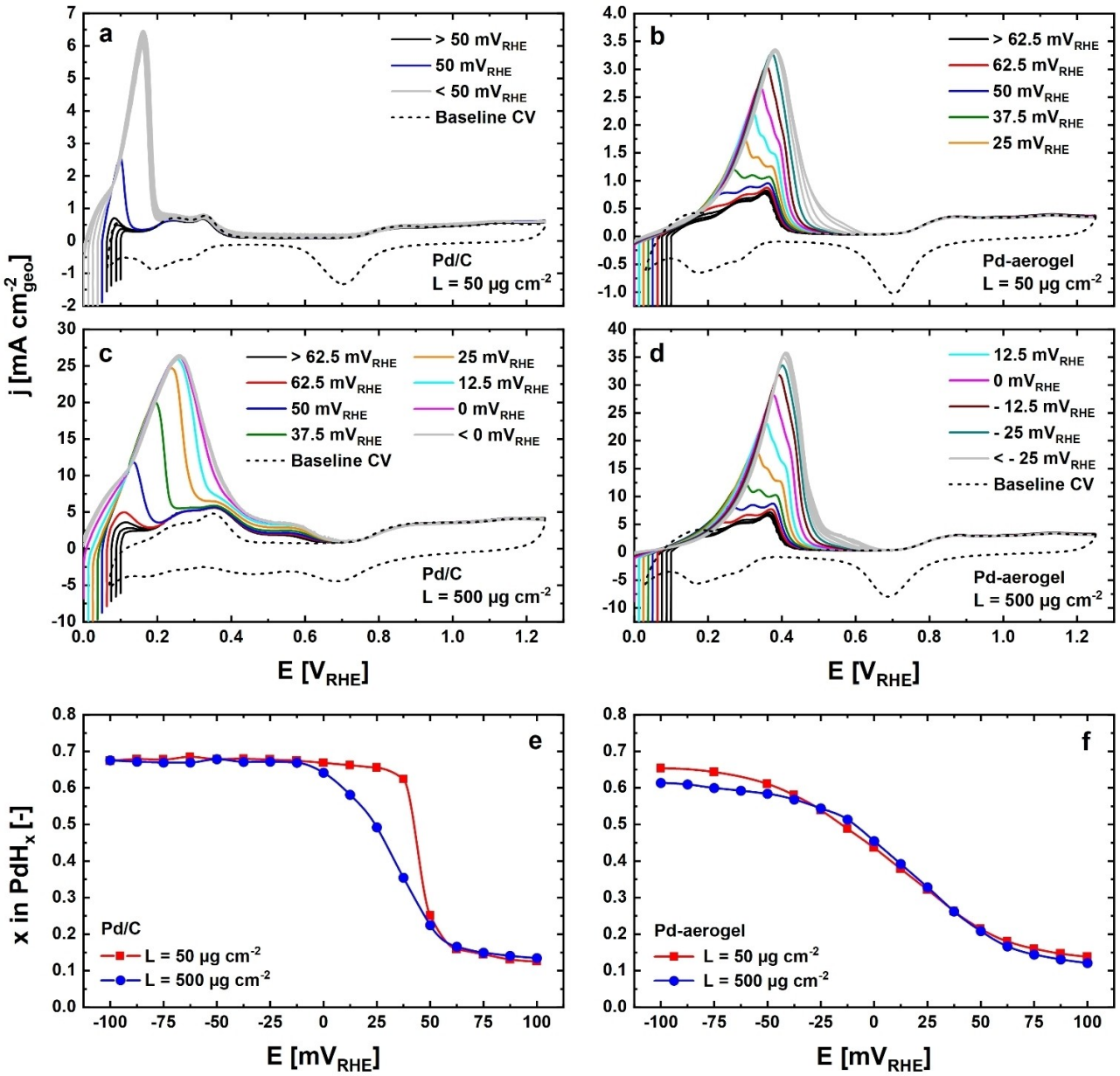

Figure 2. Positive-going linear voltammetric sweeps and subsequent baseline cyclic voltammograms recorded at 20 mV s^{-1} on Pd/C (a, c) or Pd-aerogel (b, d) electrodes after holding the potential for 60 s at the indicated values, using Pd-loadings of 50 (a, b) or 500 µg$_{Pd}$ cm$^{-2}_{geo}$ (c, d), along with the corresponding Pd-hydride stoichiometries obtained by integrating the baseline-subtracted currents recorded in the linear sweeps for Pd/C (e) or the Pd-aerogel (f). Note that the legends in b and d are supplementary to each other.

aerogel electrode has an estimated CL-thickness of ≈2 µm (see Table 1), which is only 2-fold above the ≈1 µm for which mass-transport gradients along the CL can be considered negligible.[11] This is, therefore, in agreement with the above-discussed excellent overlap of results on the Pd/C catalyst using loadings of 10 and 50 µg$_{Pd}$ cm$^{-2}_{geo}$ or thicknesses of ≈0.2 and ≈1 µm, respectively. On the other hand, the ≈100 mV potential window over which this transition from metallic Pd to β-PdH$_x$ takes place in the aerogel's RDE tests appears to be broader than the ≈50 mV needed for this in the in situ XAS measurements (cf. Figure 1a). This inconsistency could be caused by the differences in the durations of the potential holds used in each configuration (i.e., 10 vs. 1 min for in situ XAS vs. RDE, respectively). This was confirmed by performing additional RDE measurements at a potential of 25 mV$_{RHE}$ and with different hold durations, in which we found that the Pd-aerogel only attains a fully equilibrated β-hydride stoichiometry (i.e., PdH$_{\approx 0.6}$) after 300 s (see Figure S9b). This simultaneously indicates that, in contrast to the mixed α-/β-hydride phase found at 50 mV$_{RHE}$ on Pd/C, the stoichiometries found between 50 and −50 mV$_{RHE}$ after potential holds of 60 s in the Pd-aerogel (Figure 2f) do not constitute equilibrium states but rather a hydride phase that

would have likely equilibrated as β-PdH_x after longer potential holds.

This detailed comparison between the potential-dependent hydride stoichiometries of low-loaded Pd/C vs. Pd-aerogel CLs, unaffected by ion-/mass-transport limitations (cf. Figures 2e vs. f, respectively) unveils that these two materials feature significant differences in their transitions between metallic Pd and β-PdH_x states. We hypothesize that these discrepancies between the two materials stem from intrinsic differences among the hydride-formation mechanisms in their nanostructures. In this regard, one must bear in mind that these RDE measurements entail similar Pd-loadings and ECSAs (i.e., a comparable number of total Pd-atoms and H-adsorption/-desorption surface sites, respectively) and that the diffusion of hydrogen in the palladium lattice is reportedly fast (i.e., featuring a room temperature diffusion coefficient of $\approx 10^{-7}\,cm^2\,s^{-1}$, comparable to that of liquids-in-liquids).[23] Therefore, we believe that these discrepancies must stem from differences in the rates of the H-adsorption step preceding H-absorption, which is in turn possibly related to the nature of the specific surface facets (and corresponding H-sorption properties) featured in each of these materials.

Most importantly, the potential-dependent hydride formation trends inferred from the RDE-tests contradict those derived from the in situ XAS measurements. Specifically, while in RDE the thin-film Pd/C electrode formed the β-hydride at all potentials $< 50\,mV_{RHE}$ and featured a much narrower mixed-phase region than the Pd-aerogel, indicating a faster hydride formation in this Pd/C vs. the Pd-aerogel, the opposite rates were observed in XAS experiments (i.e., hydride formation was significantly faster for the Pd-aerogel vs. Pd/C—cf. Figures 1b and c). In this regard, the significant delay in hydride formation observed in the RDE measurement performed on a highly loaded Pd/C electrode strongly suggests that this disagreement between XAS and RDE results is entirely due to the differences in layer thickness in each technique, which become particularly detrimental for Pd/C (as opposed to the Pd-aerogel) due to the low density of the carbon support and correspondingly thick CL (see Table 1).

This strong delay in PdH_x-formation in the specific case of the highly-loaded Pd/C electrode must result from the appearance of gradients in potential and/or limitations in reactant availability along its CL-thickness.[3c,24] Regarding the latter possibility, the near-neutral phosphate buffer electrolyte used in these measurements (with a pH of 7.3) implies a low proton availability that would translate into the necessity for hydride formation to proceed through the surface-adsorbed hydrogen (H_{ads}) resulting from water autoprotolysis. Thus, to determine whether this proton availability may be at the root of the observed hydride formation delays, we performed another RDE measurement with a high loading of $500\,\mu g_{Pd}\,cm^{-2}_{geo}$, but in a N_2-saturated 0.1 M H_2SO_4 electrolyte of pH≈1 in which hydride formation should proceed through the direct adsorption of protons in the solution on the Pd-surface. The recorded LSVs and baseline CVs are displayed in Figure S10 and unveil a hydride formation trend similar to the one observed in phosphate buffer with a thin CL. Hence, the ≈6 orders of magnitude higher proton activity in this measurement compensates for the effects induced by the large CL-thickness previously found at near-neutral pH, and hints at the appearance of significant pH-gradients (and corresponding shifts in the applied potentials in the RHE scale) as a possible reason for the slower hydride formation rates observed in the measurements with a thick Pd/C CL. Consequently, our findings are particularly relevant in the context of CO_2-electroreduction studies that are systematically carried out in quasi-neutral electrolytes whose interfacial pH reportedly changes in the course of the electrochemical reactions.[6c,25]

In summary, we have found opposing trends regarding the rates of hydride formation on Pd-nanostructures as studied through in situ XAS or RDE measurements. By systematically varying the catalyst loading in the latter RDE configuration, we found that these discrepancies can be entirely ascribed to differences in each material's catalyst loadings and concomitant electrode thicknesses, whereby the bulky electrodes often used in in situ XAS measurements can significantly influence both spectroscopic and electrochemical results and possibly lead to wrong conclusions regarding the time-dependency of the studied effects. Notably, it is highly likely that our conclusions are relevant beyond the specific characterization method used herein (i.e., XAS), and therefore they should be taken into consideration in the context of any operando/in situ measurements requiring the use of highly loaded electrodes. As such, our results emphasize the importance of carrying out operando/in situ spectroscopic (as well as diffraction[26] and scattering[3a,27]) studies of electrochemical materials using electrode thicknesses entailing minimal mass- and/or ion-transport limitations, which in turn calls for a decrease of the loadings typically used in such measurements.[5i] For operando/in situ XAS measurements specifically, the recently developed flurescence-detected quick-XAS method[5i,13a,28] presents a promising alternative allowing for time-resolved studies with drastically reduced loadings, therewith minimizing the impact of ion- and mass-transport limitations on the acquired results. Most importantly, the relevance of the conclusions derived from in situ/operando measurements will be enhanced by such catalyst-loading reductions, since these are also crucial for the commercial success of most electrochemical energy conversion technologies, and can lead to changes in the performance and stability of the materials studied through these techniques.[29] On top of this, one must also bear in mind that the liquid electrolytes in which most operando characterization studies are performed entail a reaction environment significantly different from that encountered in the real devices (e.g., with regards to reactants' diffusivities and local concentrations),[7c] and that this can in turn cause discrepancies in the mechanisms at play in each media (and corresponding materials' performance and stability).[3c] Thus, further efforts should be devoted to carrying out operando work both with application-relevant, reduced catalyst loadings and in a reaction environment as close as possible to that encountered in the real device (e.g., in the

presence of humidified gaseous reactants and/or with ionomer-based electrolytes).

Acknowledgements

Funding of this project for PSI's Electrochemistry Laboratory by the Swiss National Science Foundation (SNSF, grant 200020L_178737) as well as for the Physical Chemistry group by the Deutsche Forschungsgemeinschaft (German Research Foundation) (DFG EY 16/18-2) is gratefully acknowledged. Lastly, the authors thank the SuperXAS beamline at the Swiss Light Source for the use of their facilities. Open Access funding provided by ETH-Bereich Forschungsanstalten.

Conflict of Interest

The authors declare no conflict of interest.

Data Availability Statement

The data that support the findings of this study are available from the corresponding author upon reasonable request.

Keywords: Catalyst Loading · Electrochemistry · Electrode Thickness · Palladium Hydride · Spectroscopy

[1] P. C. Vesborg, T. F. Jaramillo, *RSC Adv.* **2012**, *2*, 7933–7947.

[2] a) Q. Meyer, Y. Zeng, C. Zhao, *Adv. Mater.* **2019**, *31*, 1901900; b) W. Li, D. M. Lutz, L. Wang, K. J. Takeuchi, A. C. Marschilok, E. S. Takeuchi, *Joule* **2021**, *5*, 77–88; c) J. Li, J. Gong, *Energy Environ. Sci.* **2020**, *13*, 3748–3779.

[3] a) M. Povia, J. Herranz, T. Binninger, M. Nachtegaal, A. Diaz, J. Kohlbrecher, D. F. Abbott, B.-J. Kim, T. J. Schmidt, *ACS Catal.* **2018**, *8*, 7000–7015; b) S. Henning, L. Kühn, J. Herranz, J. Durst, T. Binninger, M. Nachtegaal, M. Werheid, W. Liu, M. Adam, S. Kaskel, A. Eychmüller, T. J. Schmidt, *J. Electrochem. Soc.* **2016**, *163*, F998–F1003; c) A. Siebel, Y. Gorlin, J. Durst, O. Proux, F. Hasché, M. Tromp, H. A. Gasteiger, *ACS Catal.* **2016**, *6*, 7326–7334; d) K. Ebner, J. Herranz, V. A. Saveleva, B.-J. Kim, S. Henning, M. Demicheli, F. Krumeich, M. Nachtegaal, T. J. Schmidt, *ACS Appl. Energy Mater.* **2019**, *2*, 1469–1479; e) A. E. Russell, A. Rose, *Chem. Rev.* **2004**, *104*, 4613–4636; f) Q. Jia, E. Liu, L. Jiao, S. Pann, S. Mukerjee, *Adv. Mater.* **2019**, *31*, 1805157.

[4] a) D. F. Abbott, D. Lebedev, K. Waltar, M. Povia, M. Nachtegaal, E. Fabbri, C. Copéret, T. J. Schmidt, *Chem. Mater.* **2016**, *28*, 6591–6604; b) M. Povia, D. F. Abbott, J. Herranz, A. Heinritz, D. Lebedev, B.-J. Kim, E. Fabbri, A. Patru, J. Kohlbrecher, R. Schäublin, *Energy Environ. Sci.* **2019**, *12*, 3038–3052; c) J. Timoshenko, B. Roldan Cuenya, *Chem. Rev.* **2021**, *121*, 882–961; d) E. Fabbri, D. F. Abbott, M. Nachtegaal, T. J. Schmidt, *Curr. Opin. Electrochem.* **2017**, *5*, 20–26.

[5] a) B. M. Tackett, J. H. Lee, J. G. Chen, *Acc. Chem. Res.* **2020**, *53*, 1535–1544; b) D. F. Gao, H. Zhou, F. Cai, D. N. Wang, Y. F. Hu, B. Jiang, W. B. Cai, X. Q. Chen, R. Si, F. Yang, S. Miao, J. G. Wang, G. X. Wang, X. H. Bao, *Nano Res.* **2017**, *10*, 2181–2191; c) J. H. Lee, S. Kattel, Z. Jiang, Z. Xie, S. Yao, B. M. Tackett, W. Xu, N. S. Marinkovic, J. G. Chen, *Nat. Commun.* **2019**, *10*, 3724; d) W. Sheng, S. Kattel, S. Yao, B. Yan, Z. Liang, C. J. Hawxhurst, Q. Wu, J. G. Chen, *Energy Environ. Sci.* **2017**, *10*, 1180–1185; e) W. Zhu, S. Kattel, F. Jiao, J. G. Chen, *Adv. Energy Mater.* **2019**, *9*, 1802840; f) J. H. Lee, B. M. Tackett, Z. Xie, S. Hwang, J. G. Chen, *Chem. Commun.* **2020**, *56*, 106–108; g) X. Li, S. Wang, L. Li, Y. Sun, Y. Xie, *J. Am. Chem. Soc.* **2020**, *142*, 9567–9581; h) Z. Weng, Y. Wu, M. Wang, J. Jiang, K. Yang, S. Huo, X.-F. Wang, Q. Ma, G. W. Brudvig, V. S. Batista, Y. Liang, Z. Feng, H. Wang, *Nat. Commun.* **2018**, *9*, 415; i) N. Diklić, A. H. Clark, J. Herranz, J. S. Diercks, D. Aegerter, M. Nachtegaal, A. Beard, T. J. Schmidt, *ACS Energy Lett.* **2022**, *7*, 1735–1740.

[6] a) T. Binninger, E. Fabbri, A. Patru, M. Garganourakis, J. Han, D. F. Abbott, O. Sereda, R. Kötz, A. Menzel, M. Nachtegaal, *J. Electrochem. Soc.* **2016**, *163*, H906–H912; b) P. Moreno-García, N. Kovács, V. Grozovski, M. de Jesús Gálvez-Vázquez, S. Vesztergom, P. Broekmann, *Anal. Chem.* **2020**, *92*, 4301–4308; c) A. Goyal, G. Marcandalli, V. A. Mints, M. T. M. Koper, *J. Am. Chem. Soc.* **2020**, *142*, 4154–4161; d) K. P. Kuhl, E. R. Cave, D. N. Abram, T. F. Jaramillo, *Energy Environ. Sci.* **2012**, *5*, 7050–7059; e) J. Herranz, A. Pătru, E. Fabbri, T. J. Schmidt, *Curr. Opin. Electrochem.* **2020**, *23*, 89–95; f) J. Herranz, J. Durst, E. Fabbri, A. Patru, X. Cheng, A. A. Permyakova, T. J. Schmidt, *Nano Energy* **2016**, *29*, 4–28; g) I. E. L. Stephens, A. S. Bondarenko, U. Grønbjerg, J. Rossmeisl, I. Chorkendorff, *Energy Environ. Sci.* **2012**, *5*, 6744–6762.

[7] a) J. S. Diercks, B. Pribyl-Kranewitter, J. Herranz, P. Chauhan, A. Faisnel, T. J. Schmidt, *J. Electrochem. Soc.* **2021**, *168*, 064504; b) R. J. K. Wiltshire, C. R. King, A. Rose, P. P. Wells, M. P. Hogarth, D. Thompsett, A. E. Russell, *Electrochim. Acta* **2005**, *50*, 5208–5217; c) T. Lazaridis, B. M. Stühmeier, H. A. Gasteiger, H. A. El-Sayed, *Nat. Catal.* **2022**, *5*, 363–373.

[8] a) C. M. Zalitis, D. Kramer, A. R. Kucernak, *Phys. Chem. Chem. Phys.* **2013**, *15*, 4329–4340; b) Y. Seidel, A. Schneider, Z. Jusys, B. Wickman, B. Kasemo, R. Behm, *Faraday Discuss.* **2009**, *140*, 167–184; c) A. Bonakdarpour, M. Lefevre, R. Yang, F. Jaouen, T. Dahn, J.-P. Dodelet, J. R. Dahn, *Electrochem. Solid-State Lett.* **2008**, *11*, B105.

[9] A. Dutta, M. Rahaman, N. C. Luedi, M. Mohos, P. Broekmann, *ACS Catal.* **2016**, *6*, 3804–3814.

[10] H. A. El-Sayed, A. Weiß, L. F. Olbrich, G. P. Putro, H. A. Gasteiger, *J. Electrochem. Soc.* **2019**, *166*, F458–F464.

[11] a) T. J. Schmidt, H. A. Gasteiger in *Handbook of Fuel Cells—Fundamentals, Technology and Applications* (Eds.: W. Vielstich, H. A. Gasteiger, A. Lamm, H. Yokokawa), Wiley, Hoboken, **2010**; b) T. J. Schmidt, H. A. Gasteiger, G. Stäb, P. Urban, D. Kolb, R. Behm, *J. Electrochem. Soc.* **1998**, *145*, 2354–2358.

[12] S. Czioska, A. Boubnov, D. Escalera-López, J. Geppert, A. Zagalskaya, P. Röse, E. Saraçi, V. Alexandrov, U. Krewer, S. Cherevko, J.-D. Grunwaldt, *ACS Catal.* **2021**, *11*, 10043–10057.

[13] a) K. Ebner, A. H. Clark, V. A. Saveleva, G. Smolentsev, J. Chen, L. Ni, J. Li, A. Zitolo, F. Jaouen, U. I. Kramm, T. J. Schmidt, J. Herranz, *Adv. Energy Mater.* **2022**, *12*, 2103699; b) M. Rüscher, A. Herzog, J. Timoshenko, H. S. Jeon, W. Frandsen, S. Kühl, B. Roldan Cuenya, *Catal. Sci. Technol.* **2022**, *12*, 3028–3043; c) S.-C. Lin, C.-C. Chang, S.-Y. Chiu, H.-T. Pai, T.-Y. Liao, C.-S. Hsu, W.-H. Chiang, M.-K. Tsai, H. M. Chen, *Nat. Commun.* **2020**, *11*, 3525.

[14] R. Feenstra, R. Griessen, D. G. de Groot, *J. Phys. F* **1986**, *16*, 1933–1952.

[15] A. Rose, S. Maniguet, R. J. Mathew, C. Slater, J. Yao, A. E. Russell, *Phys. Chem. Chem. Phys.* **2003**, *5*, 3220–3225.

[16] a) Q. Chang, J. Kim, J. H. Lee, S. Kattel, J. G. Chen, S.-I. Choi, Z. Chen, *Small* **2020**, *16*, 2005305; b) A. Rose, O. South, I.

Harvey, S. Diaz-Moreno, J. R. Owen, A. E. Russell, *Phys. Chem. Chem. Phys.* **2005**, *7*, 366–372; c) J. S. Diercks, M. Georgi, J. Herranz, N. a. Diklić, P. Chauhan, A. H. Clark, R. Hübner, A. Faisnel, Q. Chen, M. Nachtegaal, A. Eychmüller, T. J. Schmidt, *ACS Appl. Energy Mater.* **2022**, *5*, 8460–8471.

[17] a) M. Georgi, B. Klemmed, A. Benad, A. Eychmüller, *Mater. Chem. Front.* **2019**, *3*, 1586–1592; b) M. Georgi, Ph.D. thesis, TU Dresden **2021**.

[18] T. Mittermeier, A. Weiß, H. A. Gasteiger, F. Hasché, *J. Electrochem. Soc.* **2017**, *164*, F1081–F1089.

[19] a) J. S. Diercks, J. Herranz, M. Georgi, N. Diklić, P. Chauhan, K. Ebner, A. H. Clark, M. Nachtegaal, A. Eychmüller, T. J. Schmidt, *ACS Catal.* **2022**, *12*, 10727–10741; b) P. Chauhan, K. Hiekel, J. S. Diercks, J. Herranz, V. A. Saveleva, P. Khavlyuk, A. Eychmüller, T. J. Schmidt, *ACS Mater. Au* **2022**, *2*, 278–292.

[20] P. Millet, R. Ngameni, *Electrochim. Acta* **2011**, *56*, 7907–7915.

[21] D. R. Lide, *CRC Handbook of Chemistry and Physics*, 87th ed., Taylor and Francis, Boca Raton, **2007**.

[22] Y. Liu, C. Ji, W. Gu, D. R. Baker, J. Jorne, H. A. Gasteiger, *J. Electrochem. Soc.* **2010**, *157*, B1154.

[23] a) S. Dekura, H. Kobayashi, K. Kusada, H. Kitagawa, *ChemPhysChem* **2019**, *20*, 1158–1176; b) S. Hara, A. Caravella, M. Ishitsuka, H. Suda, M. Mukaida, K. Haraya, E. Shimano, T. Tsuji, *J. Membr. Sci.* **2012**, *421–422*, 355–360; c) F. A. Lewis, *Platinum Met. Rev.* **1982**, *26*, 121–128; d) P. Millet, *Electrochem. Commun.* **2005**, *7*, 40–44; e) E. Seymour, R. Cotts, W. D. Williams, *Phys. Rev. Lett.* **1975**, *35*, 165.

[24] K. Neyerlin, W. Gu, J. Jorne, H. A. Gasteiger, *J. Electrochem. Soc.* **2007**, *154*, B631.

[25] a) M. R. Singh, Y. Kwon, Y. Lum, J. W. Ager III, A. T. Bell, *J. Am. Chem. Soc.* **2016**, *138*, 13006–13012; b) F. Zhang, A. C. Co, *Angew. Chem. Int. Ed.* **2020**, *59*, 1674–1681; *Angew. Chem.* **2020**, *132*, 1691–1698.

[26] a) A. T. Landers, H. Peng, D. M. Koshy, S. H. Lee, J. T. Feaster, J. C. Lin, J. W. Beeman, D. Higgins, J. Yano, W. S. Drisdell, R. C. Davis, M. Bajdich, F. Abild-Pedersen, A. Mehta, T. F. Jaramillo, C. Hahn, *Chem. Mater.* **2021**, *33*, 5872–5884; b) A. L. Bugaev, O. A. Usoltsev, A. Lazzarini, K. A. Lomachenko, A. A. Guda, R. Pellegrini, M. Carosso, J. G. Vitillo, E. Groppo, J. A. van Bokhoven, A. V. Soldatov, C. Lamberti, *Faraday Discuss.* **2018**, *208*, 187–205; c) B. Ingham, M. F. Toney, S. C. Hendy, T. Cox, D. D. Fong, J. A. Eastman, P. H. Fuoss, K. J. Stevens, A. Lassesson, S. A. Brown, M. P. Ryan, *Phys. Rev. B* **2008**, *78*, 245408.

[27] a) T. Binninger, R. Mohamed, A. Patru, K. Waltar, E. Gericke, X. Tuaev, E. Fabbri, P. Levecque, A. Hoell, T. J. Schmidt, *Chem. Mater.* **2017**, *29*, 2831–2843; b) J. Schröder, J. Quinson, J. K. Mathiesen, J. J. Kirkensgaard, S. Alinejad, V. A. Mints, M. Arenz, *J. Electrochem. Soc.* **2020**, *167*, 134515.

[28] A. H. Clark, P. Steiger, B. Bornmann, S. Hitz, R. Frahm, D. Ferri, M. Nachtegaal, *J. Synchrotron Radiat.* **2020**, *27*, 681–688.

[29] a) S. M. Alia, S. Stariha, R. L. Borup, *J. Electrochem. Soc.* **2019**, *166*, F1164; b) A. Kongkanand, M. F. Mathias, *J. Phys. Chem. Lett.* **2016**, *7*, 1127–1137.

Manuscript received: November 11, 2022
Accepted manuscript online: February 7, 2023
Version of record online: March 13, 2023